Available online at www.sciencedirect.com
ScienceDirect
Ceramics International 37 (2011) 2335–2345
CERAMICS INTERNATIONAL
www.elsevier.com/locate/ceramint

Hot elastic modulus of Al_2O_3–SiC–SiO_2–C castables

A.P. Luz [a,*], M. Huger [b], V.C. Pandolfelli [a]

[a] Materials Engineering Department, Federal University of São Carlos, Rod. Washington Luiz, km 235, São Carlos, SP, C.P. 676, CEP 13565-905, Brazil
[b] Groupe d'Etude des Matériaux Hétérogènes (GEMH), ENSCI, 47 à 73, Avenue Albert Thomas, 87065 Limoges, France

Received 16 April 2010; received in revised form 15 January 2011; accepted 20 March 2011
Available online 27 May 2011

Abstract

This work discusses an investigation of the hot elastic modulus and crack generation of two Al_2O_3–SiC–SiO_2–C castable compositions throughout two thermal cycles in an oxidizing atmosphere. A high temperature ultrasonic technique carried out using a long bar mode, thermogravimetric, X-ray diffraction, apparent porosity analyses and thermodynamic calculations were evaluated in order to understand the results. Significant changes in the castables' elastic modulus values were observed with temperature, which were related to the decomposition of hydrated phases, antioxidant reactions, changes in the liquid phase viscosity, and formation and closure of microcracks in the castable microstructure. The results attained are fundamental for providing data for thermo-mechanical computing simulations by finite element analyses and for the design of large refractory structures, such as blast furnace runners for the steel industry.

Keywords: Elastic modulus; Carbon containing castables; Antioxidants

1. Introduction

The difference between Young's or elastic modulus (E) of metals, ceramics and polymers is related to the types of atomic bonds present in these three classes of materials [1]. From the scientific point of view, the elastic constants can be expressed as a second order derivative of the interatomic potentials, providing information about the material atomic bond strength. For multiphase composites, such as refractory castables, elastic constants are sensitive to the phase changes and microstructural transformations [2].

Elastic modulus can be measured using either static or dynamic tests. The three most common ways of measuring the static E value of refractories are by tensile, compression and bending tests [3–5]. Dynamic and non-destructive methods (such as the resonant technique, ultrasonic echography, etc.) have the added advantage of keeping the integrity of the material after taking the measurement [6–10]. Ultrasonic waves used in these tests are derived from mechanical vibration with frequencies higher than the audible domain, ranging from 20 kHz to hundreds of MHz [11]; with their propagation velocity depending on the elastic properties and density of the chosen environment. Ultrasonic methods are often used to evaluate the elastic modulus of heterogeneous materials due to their simplicity and accuracy. However, for multiphase refractories, the high attenuation of the acoustic waves generated by the various phases present affects the quality of the measurements, especially at high temperatures. Thus, the use of a configuration known as ''long bar mode'', with a wave frequency of about 150 kHz, is required in order to evaluate refractory castable compositions [11].

The main purpose of using the ultrasonic long bar mode echography test is to follow the evolution of the elastic modulus, which depends on the intrinsic elastic properties of constituents and the damage of the material [12]. The essential condition of this type of test configuration states that the side dimensions (d) of the prismatic sample must be small (i.e., samples presenting height and width in the range of 5–15 mm) when compared to the wave length (λ) of the ultrasonic vibration (typical values are $d/\lambda = 0.2$).

According to the literature, complex materials such as carbon containing refractories could present atypical elastic modulus behavior due to temperature [7,13]. For example, after thermal treatment at 1000 °C, Al_2O_3–C refractories have a complex microstructure consisting of Al_2O_3 coarse grains and graphite flakes in a matrix bonded by carbon. Their high

* Corresponding author. Tel.: +55 16 33518253; fax: +55 16 33615404.
E-mail address: ana_light@uol.com.br (A.P. Luz).

0272-8842/$36.00
doi:10.1016/j.ceramint.2011.05.094

thermal conductivity and lower thermal expansion make this material a good option to use in iron making processes. However, the elastic modulus of the pre-fired Al_2O_3–C refractory shows a non-linear and irreversible behavior (Fig. 1) where the large increase in elastic modulus from 450 °C to 650 °C can be associated to the closure of interparticle gaps and cracks due to the thermal expansion mismatch between coarse grains and the fine matrix particles [13]. During the cooling step (below 650 °C), the E value decrease is due to decoherences and crack opening [13]. The hysteresis phenomenon of the elastic modulus is the object of some studies, with efforts being made to better understand and explain the mechanisms responsible for this effect [14–16].

Macroscopic properties of complex materials are difficult to understand by traditional test methods. In fact, the behavior of refractories is closely related to the role of each component and to the interaction among several phases of the composition [11].

The scientific literature only contains a small amount of research focusing on the determination of the elastic behavior of MgO–C and Al_2O_3–C refractories due to the high temperature [7,13], with no studies involving high carbon containing castables of complex systems, such as Al_2O_3–SiO_2–SiC–C. This work evaluates the elastic modulus and crack generation in high carbon containing refractory castables. Two Al_2O_3–SiO_2–SiC–C castable compositions containing 10 wt.% carbon have been analyzed throughout two thermal cycles in an oxidizing atmosphere in order to evaluate the effectiveness of the antioxidant agents and possible damage caused by the oxidation process. When used in blast furnace runners, these castables are exposed to different working environment atmospheres: oxidizing (upper surface) and reducing (surface below the air–liquid interface). The wear mechanism of carbon containing refractories can be described by a two-step process: (a) oxidation of carbon at temperatures above 600 °C and (b) corrosion by molten metal and slags. In order to understand the E evolution of the evaluated castables, the high temperature ultrasonic technique results were correlated with those provided by thermogravimetric, X-ray diffraction, apparent porosity analyses and thermodynamic calculations.

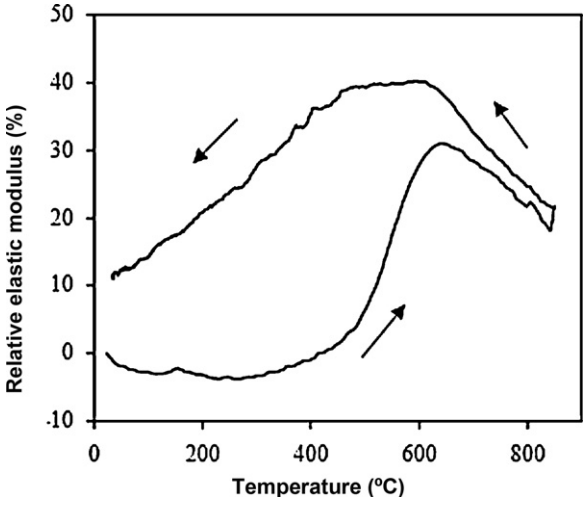

Fig. 1. Elastic modulus profile versus temperature for an Al_2O_3–C refractory [13].

2. Experimental procedure

2.1. Castable compositions

Two Al_2O_3–SiO_2–SiC–C refractory castables containing three carbon sources (coke, pitch and carbon black) and different antioxidants (Si, B_4C and sodium borosilicate glass [17]) were designed according to the Andreasen packing model ($q = 0.21$ – composition given in Table 1). The formulations consisted of a matrix with fine particles ($d < 75$ μm, including 2.0 wt.% of calcium aluminate cement) and coarse aggregates ($d < 4.75$ mm). The dispersion of the castables was carried out using an electrosteric dispersant (0.2 wt.%, Darvan-7S, R.T. Vanderbilt, Norwalk, CT) and a non-ionic surfactant (HLB = 8, 4.0 mg/m^2) as wetting agents for the carbon sources.

During the processing step, the dry powders of each castable composition were mixed for 5 min in a rheometer developed for refractory castable mixing [18] in order to attain a homogenized material. After that, water, surfactant and a dispersant were added to the mixture. All compositions were molded into 150 mm × 15 mm × 15 mm prismatic samples and cured at 50 °C in a humid environment (R.H. ≈ 100%) for 12 h, then dried at 110 °C for 24 h.

2.2. Elastic modulus

The elastic modulus profile of the carbon containing castables was evaluated using an ultrasonic technique in a long bar mode. Fig. 2 presents a sketch of the experimental setup used for high temperature ultrasonic echography measurements. According to this experimental setup, the reflection of the pulse at the wave-guide and the alumina guide

Table 1
Al_2O_3–SiO_2–SiC–C castable compositions.

Raw materials	10C (wt.%)	10SBC (wt.%)
Brown fused alumina ($d = 4/10 – 200$ mesh)[a]	44.0	44.0
SiC (EC6R, $d = 6/10 – 200$ mesh)[b]	20.0	20.0
Calcined alumina (CL370C, $d_{50} = 4$ μm)[c]	21.0	16.0
Cement (Secar71, $d_{50} = 6$ μm)[d]	2.0	2.0
Silica fume (971-U, $d < 2$ μm)[e]	1.0	1.0
Silicon (Silgrain, $d_{50} = 25$ μm)[e]	–	5.0
Sodium borosilicate glass ($d_{50} = 7$ μm)[f]	–	1.0
Boron carbide ($d_{50} = 25$ μm)[g]	2.0	1.0
Pitch ($d < 125$ μm)[h]	5.0	5.0
Carbon black ($d < 2$ μm)[h]	3.0	3.0
Coke ($d < 200$ μm)[h]	2.0	2.0
Water	5.2	6.3

[a] Elfusa (Brazil).
[b] Treibacher (Brazil).
[c] Almatis (USA).
[d] Kerneos (França).
[e] Elkem Refractories (Norway).
[f] Ferro Enamel (Brazil).
[g] China Brasilis (China).
[h] Unimetal, Cabot and Nacional de Grafite (Brazil).

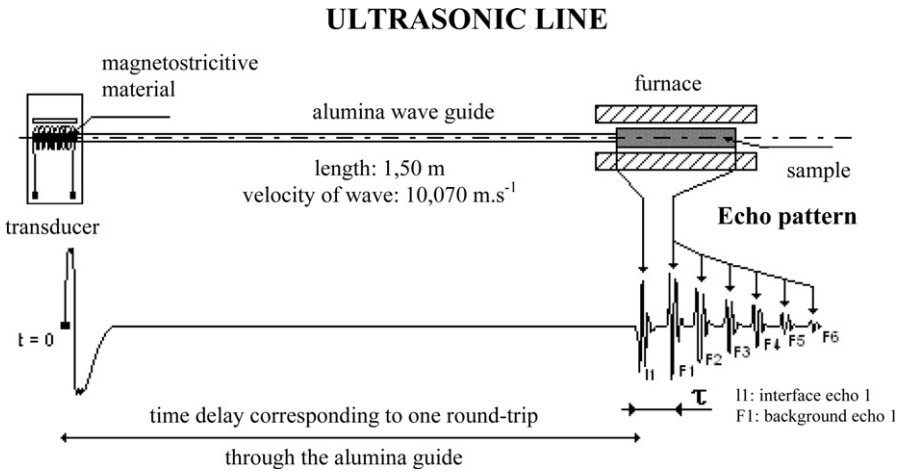

Fig. 2. Ultrasonic elastic modulus measurement at high temperature.

sample interfaces gives the first echo, and the reflection at the end of the sample the second one. The measurement of the time between two echos (t) is related to the wave velocity and the elastic modulus (E) of the material by the following equation [15]:

$$E = \rho\left(\frac{2L}{t}\right)^2 \quad (1)$$

where L and ρ are the sample length and density, respectively.

In the experimental setup of Fig. 2, an ultrasonic pulse is generated by a ferromagnetic nickel bar transducer placed in the cold zone of the system. Nickel was used due to its similar value of acoustic impedance when compared with alumina and a 40 kHz transducer was selected for elastic modulus measurements.

During the measurements, the ultrasonic pulse was transmitted from the transducer to the castable sample using an alumina wave guide. The ferromagnetic bar (diameter = 5 mm) was attached to one of the edges of the wave guide using cyanoacrylate glue. Refractory cement (Cotronics 903HP, USA) was used to attach the castable sample to the other edge of the same guide.

The experiments were carried out for two thermal cycles between 20 °C and 1500 °C under oxidizing atmosphere at heating and cooling rates of 5 °C min^{-1}. In this work, only the results attained in an oxidizing atmosphere will be presented, but the experiments carried out under inert gas flux (argon flux = 85 mL/min, heating/cooling rates = 5 °C min^{-1} and temperature cycle = 20–1500 °C) were used to understand and analyze the data presented and discussed here.

2.3. Additional measurements

The weight changes of the B_4C and Si antioxidants and of the carbon sources mixture [coke (partially crystallized), pitch and carbon black (amorphous)] were recorded as a function of temperature by thermogravimetric experiments. The aim of these tests was to detect the beginning of the carbon oxidation and antioxidant reactions with O_2 and CO. Reactions occurring in B_4C, Si, and a mixture of carbon powders were evaluated between room temperature and 1200 °C at a heating rate of 5 °C min^{-1}.

The refractory phases were identified using an X-ray diffraction technique. For this purpose, the castable samples were fired at the temperatures of 600 °C, 1200 °C and 1500 °C for 5 h in oxidizing atmosphere, then crushed and milled in a WC shatter box. The resulting powders were analyzed for crystalline phases by X-ray using an INEL CPS120 equipment in the 2θ range of 5–80° with Cu Kα radiation.

The apparent porosity of the refractory samples after firing at 400 °C, 600 °C, 800 °C, 1000 °C 1200 °C, 1400 °C and 1500 °C for 5 h was measured by the Archimedes method (ASTM C380-00), using water as the immersion liquid.

Additionally, in order to better understand the phase transformations of the carbon containing castables, thermodynamic calculations were predicted using FactSage™ software – version 6.0 (Thermfact and GTT-Technologies). The use of this tool is required due to the complexity of the phases formed at high temperatures and the difficulties of identifying and determining their amount in the castable microstructure. This software uses a series of modules that access thermodynamic databases and do various calculations. The databases used in this study were Fact53, FToxid and SGTE. The equilibrium phases were predicted using the Equilib module and considered the following phases: gas, slag or liquid; assuming both stoichiometric solids and non-stoichiometric solid-solutions. These calculations involved the thermal treatments of 10C and 10SBC castables between 400 and 1500 °C in the presence of a total of 7.8×10^{-2} moles of oxygen in the system.

3. Results and discussion

Most of the microstructural (densification, phase changes, crystallization, etc.) and damage evolution (microcracking, generation of pores, etc.) in solid materials are related to changes in the elastic modulus. Consequently, E measurements at high temperatures can be used to evaluate the thermomechanical behavior of the refractory castables.

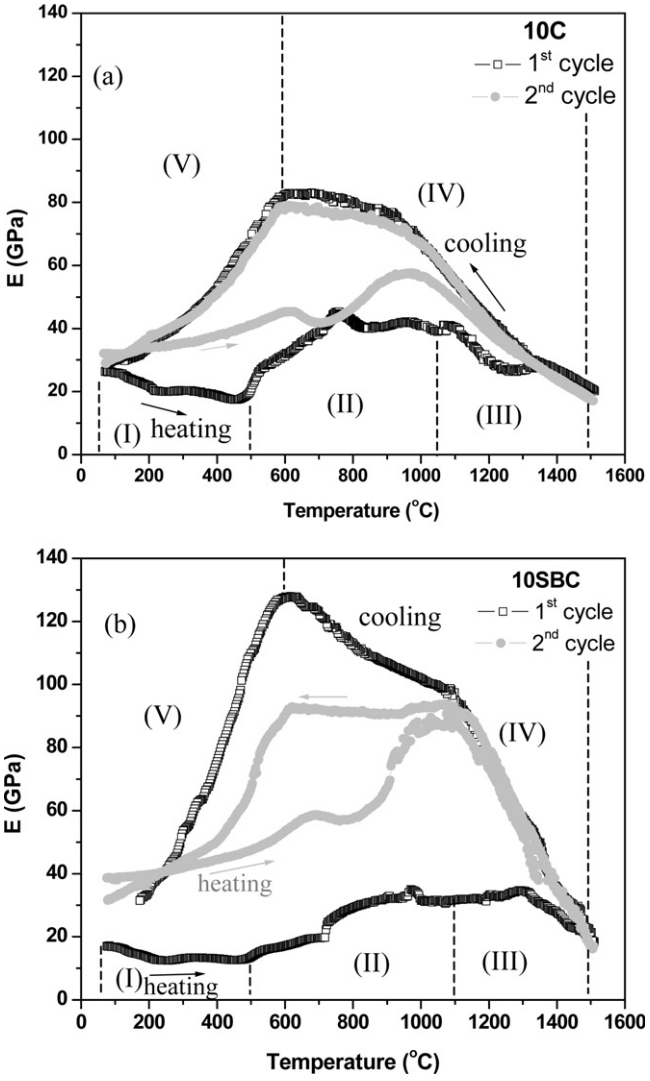

Fig. 3. Elastic modulus evolution as a function of temperature, under oxidizing atmosphere ($pO_2 = 0.21$ atm): (a) 10C and (b) 10SBC samples obtained after curing and drying steps.

Fig. 3 presents the *E* results of the high carbon containing castables collected throughout two thermal cycles up to 1500 °C in an oxidizing atmosphere. The evaluated samples were previously cured at 50 °C and dried at 110 °C. Consequently, the water withdrawal, carbon and cement phase changes affected the first heating curve and the initial *E* values at room temperature (10SBC = 18 GPa and 10C = 26 GPa).

Carbon from pitch can be graphitized at elevated temperatures and the coke yield increased by the addition of carbon black or other carbonaceous materials [19]. In general, the yield of carbon is determined by the amount of volatile carbon containing species that are generated and the initial carbon content. Pitch was the main carbon source added to the 10C and 10SBC castable samples (5 wt.%), and during its pyrolysis (between 400 and 550 °C), the formation of a liquid crystal phase or mesophase in the castable structure can give rise to a graphitizable carbon. These transformations may directly affect the *E* values of the refractories, with new carbon bonds forming at the beginning of the first heating treatment.

All elastic modulus curves presented a hysteresis, which is usual because of crack closures and opening mechanisms that occur during heating and cooling cycles in materials comprising coarse grains [9]. The following sections present and discuss the castables' reactions and transformations that influenced the elastic modulus behavior.

3.1. Decomposition of the hydrated phases and carbon transformations – region I (room temperature up to 500 °C)

The initial drop of the *E* values from room temperature up to 500 °C in the first heating cycle is associated with the loss of chemically bonded water of the cement hydrated phases [20] and the development of mesophase derived from the carbon transformations [19]. The mesophase usually is formed at temperatures close to 400 °C, with a semi-coke phase generated at temperatures of 500–550 °C, although these changes also strongly depend on the heating rate.

The water loss and the cement phase changes result in voids (pores) in the structure of the refractories, causing a decrease in the elastic modulus up to 500 °C. Furthermore, for the 10SBC samples, a higher water content was required (6.2 wt.%) when compared with the 10C ones (5.2 wt.%). Low *E* values (attained between room temperature and 500 °C in oxidizing conditions) of the 10SBC castable were related to the higher water demand used in processing, and consequently, higher samples porosity (porosity after curing: 10C = 12.1 ± 0.4% and 10SBC = 14.4 ± 0.6%).

Some experiments performed in argon (results not shown here) also presented the drop of the elastic modulus in the same temperature range, indicating that the *E* behavior was the same in both atmospheres.

3.2. Carbon oxidation and antioxidants performance – region II (from 500 °C up to 1100 °C)

At temperatures higher than 500 °C, the elastic modulus is affected by the cement phase transformations, antioxidants behavior, and carbon oxidation. After the decomposition of the CAH_{10}, C_2AH_8, AH_3 and C_3AH_6 hydrates (where C = CaO, A = Al_2O_3, H = H_2O) in the temperature range of 100–400 °C, new cement phases can be generated, such as CH and $C_{12}A_7H$. With the increase of the temperature, CH and $C_{12}A_7H$ will decompose at 450 °C and 750 °C, respectively, and CA crystallization will take place between 900 and 1000 °C [1]. This latter transformation (Eq. (2)) is followed by a slight volumetric shrinkage ($\Delta V/V = -1.14\%$), leading to the decrease of the elastic modulus of the samples.

$$C_{12}A_7 + 5A \rightarrow 12CA \quad (2)$$

At higher temperatures (1100–1400 °C), expansive reactions related to CA alumina enrichment can generate CA_2 and CA_6 phases, which will affect the elastic properties of the carbon containing castables.

Carbonization of the semi-coke phase resulting from the carbon sources reactions will have a critical effect on the castable properties between 600 °C and 800 °C, with compo-

sites containing pitch in their matrix tending to show an overall expansion due to the evolution of the volatile matter [19]. The matrix expansion will allow the interaction of the carbon with the gases of the environment, inducing the carbon oxidation and decreasing the E values.

Si, B_4C and sodium borosilicate glass additives in 10SBC interact with oxygen or $CO_{(g)}$ and the castable components at different temperatures, impacting the refractory E behavior in distinct ways. It is also known that there is no single effective antioxidant for all castable compositions and situations. Nevertheless, recent results have indicated that the use of a blend of metallic and non-metallic antioxidants is very efficient at preventing carbon oxidation [17,21].

10C castable contains only B_4C as an antioxidant in its composition. Boron-based additives act to block the open pores, reducing the oxidation of carbon by forming oxide and liquid phases [17]. When analyzing 10C in Fig. 3a (first cycle), E reached a maximum between 500 °C and 750 °C. This behavior can be associated with the reaction of B_4C with oxygen or CO, resulting in liquid phase generation (B_2O_3) and carbon deposition at the castable surface.

$$B_4C_{(s)} + 3O_{2(g)} \leftrightarrow 2B_2O_{3(l)} + C_{(s)}, \quad \Delta G_{500\,^\circ C} = -2077\,\text{kJ} \tag{3}$$

$$B_4C_{(s)} + 6CO_{(g)} \leftrightarrow 2B_2O_{3(l)} + 7C_{(s)}, \quad \Delta G_{500\,^\circ C} = -997\,\text{kJ} \tag{4}$$

The thermogravimetric results of the B_4C in air (Fig. 4a) showed that at 500 °C, the increase in the initial weight of this carbide indicates the beginning of the B_2O_3 generation at the surface of the B_4C particles. The weight reaches its maximum value at 700 °C, which corresponds to a 18.3 wt.% increase. However, at higher temperatures the weight loss might be associated to partial B_2O_3 volatilization and carbon oxidation (secondary carbon produced by the initial reactions between B_4C and O_2 or CO).

$$2C_{(s)} + O_{2(g)} \rightarrow 2CO_{(g)}, \quad \Delta G_{500\,^\circ C} = -360\,\text{kJ} \tag{5}$$

Thermodynamic equilibrium diagrams of B_4C and Si as a function of temperature and oxygen partial pressure were prepared using the FactSage software as shown in Fig. 5. It is observed in Fig. 5a that depending on the oxygen partial pressure of the firing atmosphere, the carbon provided by B_4C (Eq. (3)) will be oxidized, generating some gaseous products such as CO and CO_2. Furthermore, thermodynamic calculations indicated that B_2O_3, BO_2 and BO as gas species were in equilibrium with liquid B_2O_3. However, boron containing gases corresponded to a small fraction of the total amount of the boron present.

From the thermodynamic plots in Fig. 5, one would expect that B_4C will act efficiently as an antioxidant at temperatures through 1000 °C, where its performance becomes influenced by oxygen partial pressure [21]. On the other hand, the carbon sources mixture (coke, pitch and carbon black) investigated in the castables began to oxidize close to 500 °C (Fig. 4b and Eq. (5)). The carbon oxidation of the refractory material

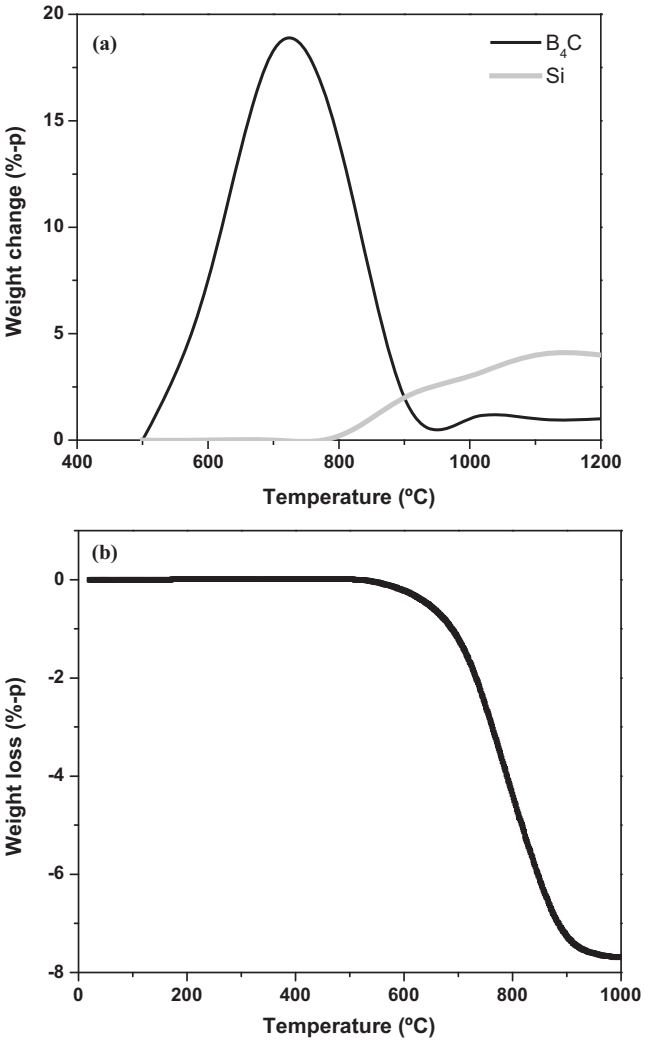

Fig. 4. (a) Pure B_4C and Si metallic weight change and (b) weight loss of the carbon sources mixture added to the studied castables (coke, pitch and carbon black) as a function of the temperature ($pO_2 = 0.21$ atm and heating rate = 5 °C min^{-1}).

increases the CO content and can induce $B_2O_{3(l)}$ generation for the 10C and 10SBC castables, according to Eq. (4).

A thin oxidized layer at the samples surface was detected and the antioxidants performance inhibited the oxygen interaction and further carbon oxidation. Regarding the thermodynamic calculations and the XRD results, it was found out that the resulting castable phases were associated with transformations carried out in an environment containing a very limited oxygen partial pressure. Thus, in order to match the experimental results with the thermodynamic predictions, the phase evolution was simulated in FactSage™ considering a high shortage of oxygen (7.8×10^{-2} moles of oxygen were added to the system as an initial reagent – $pO_2 < 10^{-24}$ atm, Fig. 6). According to the results, liquid B_2O_3 can react with alumina of the castables, resulting in the formation of $(Al_2O_3)_9(B_2O_3)$ as a stable compound from 400 to 1200 °C. These results also show the likelihood of SiC oxidation (Eq. (6)) and $CaAl_2Si_2O_8$ (anorthite – Eq. (7)) generation for the 10C composition. Based on the thermodynamics, in a CO

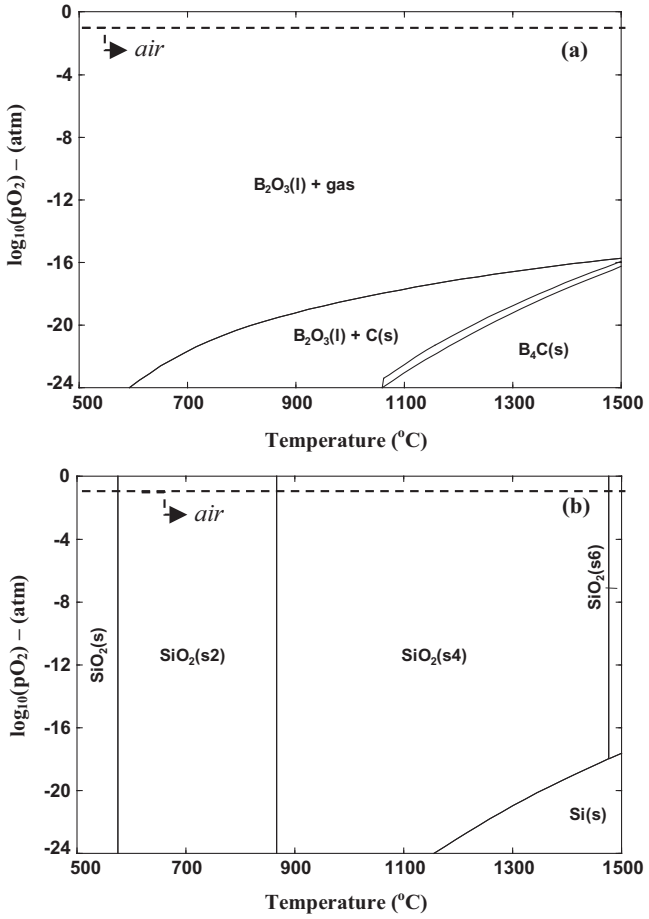

Fig. 5. Phase equilibrium diagrams presenting the (a) B_4C and (b) Si phase evolution as a function of temperature and oxygen partial pressure.

environment, SiC oxidation and the formation of anorthite have a favorable Gibbs energy value (negative ΔG) at 400 °C under equilibrium condition. Nevertheless, other factors such as the reaction kinetics, particle size distribution, castable permeability and oxygen partial pressure would impact these transformations under practical conditions.

$$SiC_{(s)} + 2CO_{(g)} \rightarrow SiO_2 + 3C_{(s)}, \quad \Delta G_{400\,^\circ C} = -378\,kJ \qquad (6)$$

$$CaO_{(s,l)} + 2SiO_{2(s,l)} + Al_2O_{3(s)} \rightarrow CaAl_2Si_2O_{8(s,l)}, \quad \Delta G_{400\,^\circ C} = -118\,kJ \qquad (7)$$

Thermodynamically, the reaction of SiC with CO could occur at low temperatures (Fig. 6a and b). The decrease in the initial amount of SiC [20 wt.% (Table 1) to 18 wt.%, as shown in Fig. 6] is related to the O_2 content in the system and its role in the carbon and B_4C oxidation (Eqs. (3) and (5)). Additionally, the resulting CO might still react with SiC and lead to SiO_2 and C generation (Eq. (6)). The ΔG value for Eq. (6) at 400 °C ($\Delta G = -378$ kJ) is higher than the one from Eq. (5), indicating that the interaction between SiC and CO is thermodynamically more favorable. SiO_2 can further react with CaO (from the calcium aluminate cement) and Al_2O_3 (from the castable and cement), resulting in anorthite at higher temperatures.

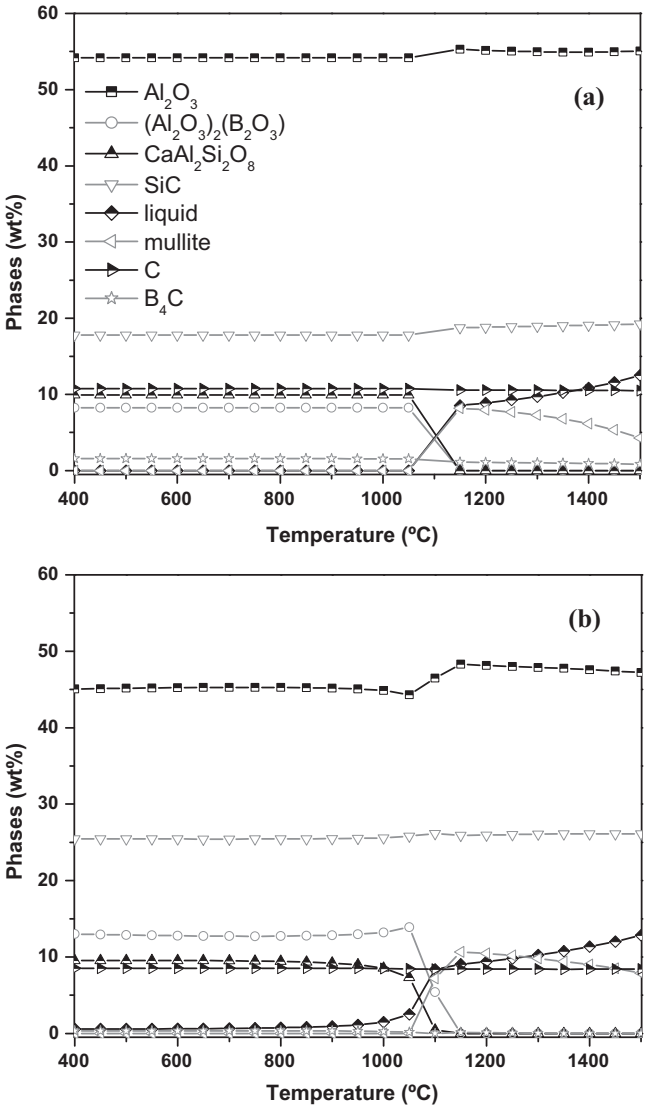

Fig. 6. Phases evolution (predicted using the FactSage software) as a function of temperature: (a) 10C and (b) 10SBC (7.8×10^{-2} moles of oxygen were added to the system to simulate a condition similar to the experimental observations).

Only SiC and B_4C oxidation and anorthite formation are predicted in the 400–1200 °C temperature range. X-ray diffraction results determined the presence of $(Al_2O_3)_9(B_2O_3)$ in the 10C castable samples thermally treated at 1200 °C (Fig. 7). However, the predicted anorthite phase ($CaAl_2Si_2O_8$) was not identified in any of the evaluated samples. Thus, it is believed that the pores filled by $B_2O_{3(l)}$ (melting point = 449 °C) and their reaction with alumina are the main phases formed, and are thought responsible for the increase in the elastic modulus of the 10C castable between 500 and 750 °C (Fig. 3a).

10SBC castable (Fig. 3b) presents a smooth continuous elastic modulus increase in the 450–1300 °C range on the initial heating due to the combined action of the three added antioxidants – boron carbide, sodium borosilicate glass and silicon (metallic). Because sodium borosilicate glass is a boron containing antioxidant, its performance should be very similar

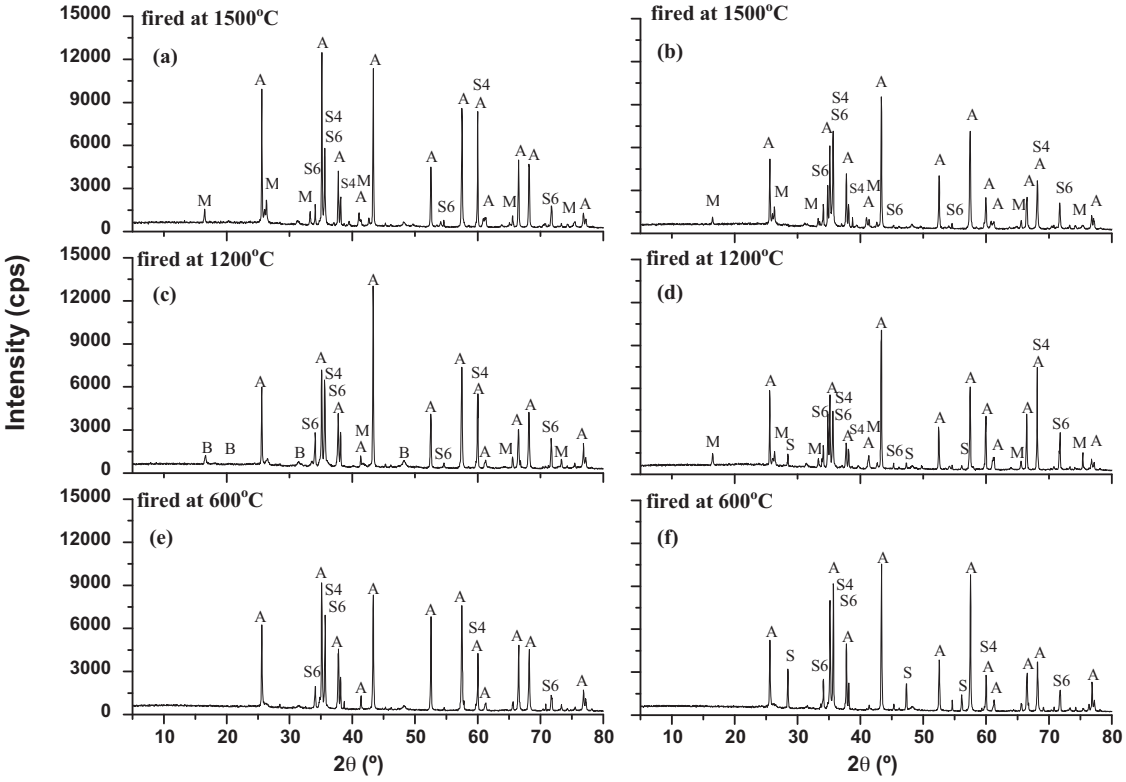

Fig. 7. X-ray diffraction of the 10C (a, c and e) and 10SBC samples (b, d and f) thermally treated in oxidizing atmosphere (pO_2 = 0.21 atm). B = $(Al_2O_3)_9(B_2O_3)$, A = Al_2O_3, S6 = SiC 6H, S4 = SiC 4H, S = silicon and M = mullite (6H and 4H are the SiC politypes).

to B_4C, with a higher amount of liquid B_2O_3 expected to be formed in 10SBC refractory samples between 450 °C and 750 °C.

Thermodynamic calculations predict that a higher amount of $(Al_2O_3)_9(B_2O_3)$ and SiC might be present in the 10SBC castable composition (Fig. 6b). The increase in SiC content from 20 wt.% (Table 1) to 26 wt.% (Fig. 6) is related to the predicted reaction involving the metallic Si and carbon on the surface and pores of the castable (Eq. (8)), which is derived from previous SiC and B_4C oxidation (Eqs. (3), (4) and (6)).

$$Si_{(s)} + C_{(s)} \leftrightarrow SiC_{(s)}, \quad \Delta G_{400\,^\circ C} = -68\,kJ \tag{8}$$

X-ray diffraction results did not indicate the presence of $(Al_2O_3)_9(B_2O_3)$ and anorthite in the 10SBC refractory, and Si could still be identified at 1200 °C. Most likely, the B_2O_3 liquid phase formed on the surface of the samples, which acted to protect the carbon particles and inhibit Si oxidation. Consequently, the Si metal additive could be found in the castable microstructure at high temperatures. The diagram shown in Fig. 5b indicates that, when Si is exposed to an environment with low oxygen partial pressure (a condition which might be found inside carbon containing refractory samples), this antioxidant does not experience oxidation at 1200 °C.

Pure metallic Si can react with O_2 in the environment at 800 °C, according to the thermogravimetric evaluation presented in Fig. 4a. Thus, the *E* increase between 800 °C and 1300 °C might also be associated to SiO_2 generation (due to Si oxidation at the samples surface) in the 10SBC castable. Experimental results presented in the literature indicate that Si can still react with C and form SiC at temperatures higher than 1100 °C (Eq. (8)) [16]. The thermodynamic calculations highlight that even at 400 °C, Eq. (8) might be possible because the Gibbs energy of this transformation is negative. Nevertheless, during the practical experiments, the reaction kinetics and the physical contact of the particles of Si and C will limit this reaction. Consequently, Si is not entirely oxidized or reacted with C up to 1200 °C, and this phase is still identified in the 10SBC composition, as shown in Fig. 7d.

SiC formed by Eq. (8) acts to prevent carbon oxidation and improves the mechanical properties of the refractories. However, at temperatures higher than 1200 °C, Si and SiC oxidation will cause an increase of liquid phases in the castable. The intensity decrease or the absence of the Si and SiC peaks in the X-ray diffraction profiles for the 10SBC sample fired at 1500 °C (Fig. 7b) pointed out that these phases reacted with O_2 or CO at this temperature. Thus, the 10SBC performance during the first heating depends on the various transformations involving the antioxidant agents.

3.3. Decrease in the liquid phase viscosity and mullite generation – region III (from 1100 °C up to 1500 °C)

Liquid phase is formed at temperatures higher than 1100 °C due to the reactions among CaO, Al_2O_3 and SiO_2, and $(Al_2O_3)_9(B_2O_3)$ (Fig. 6). With an increase in temperature, however, the liquid phase viscosity can be reduced, the volatilization of B_2O_3 increases, and carbon oxidation might

take place in the 10C and 10SBC samples. These transformations would result in a decrease of elastic modulus values at elevated temperatures. Additionally, mullite generation can also affect the E behavior above 1200 °C due to the volumetric changes during its formation (±5% [22]), which might induce some flaws and cracks in the castable microstructure. Nevertheless, further investigations are still necessary to improve the understanding of the role of mullite in elastic modulus changes at high temperatures.

Liquid formed in the castable microstructure above 1100 °C can partially fill in pores and interstices between the solid particles. Besides predicting the total amount of each phase (see Fig. 6), thermodynamic calculations also provide the mole fraction of the oxides that comprise the liquid phase formed in the castable compositions. This information for 10C and 10SBC castables is presented in Table 2.

In addition to the solid phases, the liquid composition (predicted by FactSage) and its viscosity can be estimated using the modified Urbain model [23]:

$$\eta = ATe\left(\frac{1000B}{T}\right) \tag{9}$$

where η is the viscosity in Poise, T is the temperature in Kelvin, and A and B are constants depending on the composition of the liquid. A and B are related according to the following expression:

$$\ln(A) = -0.2812B - 11.8279 \tag{10}$$

The value of B is a function of the mole fraction of SiO_2 (N) (Eq. (11)) and it can be calculated using the following equations:

$$B = B_0 + B_1N + B_2N^2 + B_3N^3 \tag{11}$$

$$B_0 = 13.8 + 39.9355\gamma - 44.04\gamma^2 \tag{12}$$

$$B_1 = 30.481 - 117.1505\gamma + 129.9978\gamma^2 \tag{13}$$

$$B_2 = -40.9429 + 234.0486\gamma - 300.04\gamma^2 \tag{14}$$

$$B_3 = 60.7619 - 153.9276\gamma + 211.1616\gamma^2 \tag{15}$$

γ represents the ratio involving the oxide components that influence the liquid behavior; whereas the compounds presented in the numerator of Eq. (16) are the ones that impact its viscosity.

$$\gamma = \frac{CaO + MgO + Na_2O + K_2O + FeO + TiO_2}{CaO + Al_2O_3 + MgO + Na_2O + K_2O + FeO + TiO_2} \tag{16}$$

This method assumes that all oxides in Eq. (12) will change their liquid viscosity depending on their content. However, B_2O_3, which is one of the main oxides present in the liquid of the 10C and 10SBC castables, is not taken into account in this model. Thus, the results generated in the calculation correspond to an approximation of the actual behavior of the formed liquid phase.

Fig. 8 plots the predicted viscosity (η) based on FactSage liquid chemistry as a function of temperature. The η values of the liquid vary from 3.8 to 1 Pa s between 1350 °C and 1500 °C. The liquid viscosity in the 10SBC composition is slightly higher than the 10C one due to the larger amount of SiO_2 generated by the Si and SiC oxidation. SiO_2 has a large impact on the viscosity of the liquid because Si^{4+} ions are network formers [23,24]. The decrease in the liquid phase viscosity with the increase of the temperature is one of the mechanisms related to the reduction of the elastic modulus of the refractory castables above 1350 °C (Fig. 3).

On the other hand, the main mechanism for mullite generation is silica diffusion (SiO_2 derived from the initial silica fume in the composition and from partial Si and SiC oxidation) through the liquid phase to the vicinity of the alumina grains. It is thought that Al_2O_3 diffusion is very low and can be ignored [25]. X-ray diffraction results confirmed the formation of mullite in the fired samples at 1200 °C and 1500 °C of the 10C and 10SBC castables (Fig. 7). Nevertheless, additional research is necessary to define and understand the role mullite plays in the presence of liquid phase and in the elastic modulus profile of the carbon containing castables.

Table 2
Mole fraction of the liquid phase components of the 10C and 10SBC castables for pO_2 = 0.05 atm.

Oxides	10C – mole fraction				10SBC – mole fraction			
	Temperatures (°C)							
	1350	1400	1450	1500	1350	1400	1450	1500
Al_2O_3	0.35	0.37	0.38	0.40	0.33	0.35	0.36	0.38
SiO_2	0.16	0.15	0.15	0.14	0.20	0.20	0.20	0.20
CaO	0.26	0.25	0.24	0.23	0.25	0.23	0.21	0.20
B_2O_3	0.23	0.23	0.23	0.23	0.19	0.19	0.19	0.18
Na_2O	–	–	–	–	0.01	0.01	0.01	0.01
$NaAlO_2$	–	–	–	–	0.02	0.02	0.02	0.02
$NaBO_2$	–	–	–	–	0.00	0.00	0.01	0.01

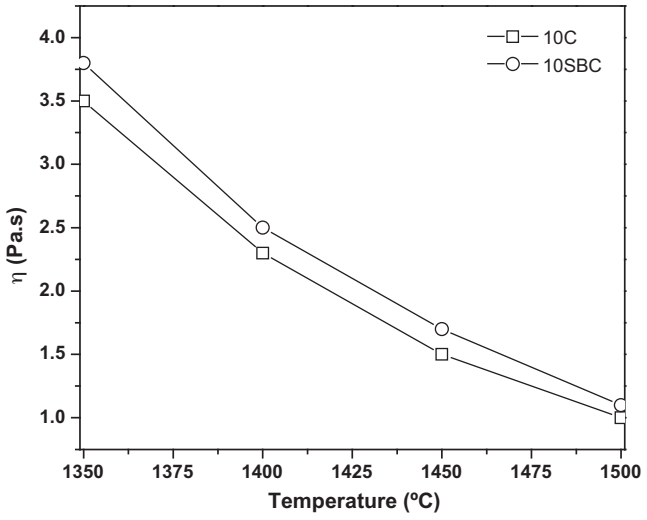

Fig. 8. Viscosity of the liquid phase formed in the 10C and 10SBC castables as a function of temperature (7.8×10^{-2} moles of oxygen were added to the system to simulate a condition similar to the experimental observations).

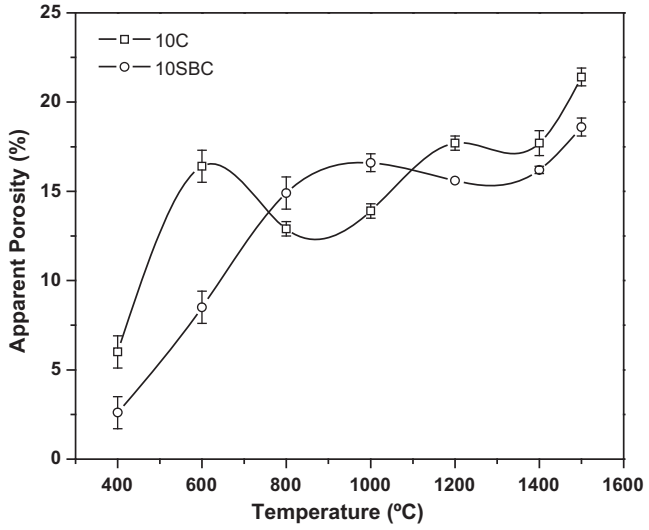

Fig. 9. Apparent porosity of the 10C and 10SBC castable samples after firing at various temperatures for 5 h in oxidizing atmosphere ($pO_2 = 0.21$ atm).

The antioxidants performance is predicted to be less effective at high temperatures, and it is expected that the carbon particles will become partially oxidized, increasing the porosity in the refractories microstructure. This effect was observed and confirmed by evaluating some castables' samples exposed to various thermal treatments carried out between 400 °C and 1500 °C in an oxidizing atmosphere. The amount of pores and flaws increased in the evaluated temperature range, mainly due to the decomposition of the hydrated phases (between room temperature and 500 °C) and carbon oxidation (Fig. 9). Pores and other flaws led to a decrease of the *E* values at high temperatures.

3.4. Increase of the liquid viscosity – region IV (from 1500 °C down to 600 °C)

During the cooling cycle, a large increase in the elastic modulus occurred from 1500 °C to 600 °C (Fig. 3) for the two castables studied. This *E* variation is related to the usual stiffening of the material when temperature decreases due to the increase in the liquid viscosity [11].

The elastic modulus curves of the 10C and 10SBC samples attained in the first cooling cycle had a distinct behavior when compared with ones collected during the heating stage. This difference can be explained by all the microstructural transformations of the castable samples and the changes between the initial phases and those generated with the increase of the temperature.

3.5. Microcracks generation – region V (from 600 °C down to room temperature)

When elastic modulus is plotted from 600 °C to room temperature, the decline of *E* values is associated with the development of flaws induced by the thermal expansion mismatch among the phases comprising the 10C and 10SBC castables' samples. This behavior is not discussed in detail here because various mechanisms can simultaneously take place on cooling cycle (micro-displacements between grains within the matrix, interfacial decoherences between phases, microcracking, etc.). Thus, even when experimental techniques are used to evaluate cracks and flaws contained in the castable samples after the elastic modulus tests, difficulties are still found and few sound conclusions can be drawn [26].

Some work in the literature evaluated refractory compositions containing only two constituents (a matrix and grains of a unique sort of aggregate) that suggested the mechanisms which are related to the thermal expansion mismatch between these phases (interfacial decoherences, microcracking, etc.) [2,8,11,26] caused the decrease in the elastic modulus. However, from a practical point of view, the evaluation of the actual castable compositions (containing various constituents, as most industrial ones) by the long bar mode can provide useful information by defining at which temperature range the embrittlement or cracks opening in the refractory's microstructure might occur.

The final elastic modulus measurement at room temperature of the castables attained after one complete (heating and cooling) cycle showed a slight increase, changing from 26 to 33 GPa for the 10C material and from 18 to 40 GPa for the 10SBC one. This is indicative that some of the initial flaws contained in the castables' microstructure were eliminated in this first thermal treatment and that some *in situ* formed phases have average elastic modulus values higher than the original raw materials of the compositions. However, further conclusions would be speculative due to the microcracking effect. It is worth noting that the highest elastic modulus was attained by the 10SBC samples (≈40 GPa) after the thermal treatments, showing good performance of the antioxidant blend.

3.6. Second thermal cycle

The elastic modulus results collected throughout the second thermal cycle (Fig. 3) had a narrower hysteresis loop than the first cycle, with the initial and final *E* values very similar to the ones after the first treatment. The lower hysteresis area indicates that the castable samples underwent less microstructural damage during the second firing. During the second heating, the changes in the refractory samples microstructure resulted in a gradual decrease in the thermal expansion mismatch, leading to a progressive elastic modulus increase. The *E* evolution from room temperature up to 600 °C might also be related to the closure of the cracks formed in the first cooling cycle, and to further generation of $B_2O_{3(l)}$, because the first cycle was carried out using a heating rate of 5 °C min^{-1}. The faster heating rate might not have allowed the oxidation reactions to reach the equilibrium condition shown in Fig. 5.

Regarding the cooling step, castable 10C showed the same *E* profile in the two curves, which supports the contention that the phase transformations of the first cycle were completed (Fig. 3). Nevertheless, during the second cooling of the 10SBC samples, no *E* change was observed over the 1200–650 °C temperature range. Various experiments using the 10C and 10SBC castable samples were carried out between 20 °C and 1500 °C and

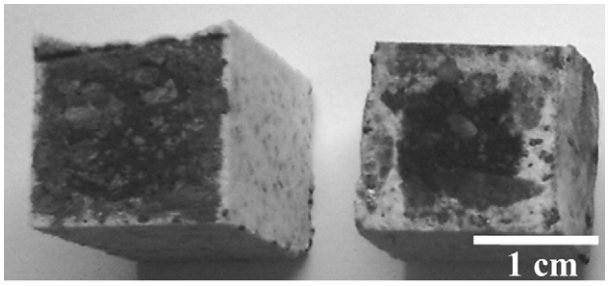

Fig. 10. Cross sections of the samples after two thermal cycles in oxidizing atmosphere ($pO_2 = 0.21$ atm).

similar reproducibility of the collected results were observed. Therefore, at the moment, the only viable explanation for this E plateau in this temperature range is a balance between the viscosity increase and crack formation, both of which occur on cooling.

In order to better compare the attained results, additional information of the hysteresis area was calculated to determine which castable had the most damage resulting from thermal treatments.

According to the hysteresis area of the elastic modulus curves (Table 3), castable 10SBC was the one which showed the highest values in the first cycle (80.454 GPa °C), and consequently, the greatest microstructure changes. Due to the action of three sorts of antioxidants, the 10SBC composition presented an unstable elastic modulus behavior during its first thermal treatment. However, this refractory also showed the lowest hysteresis area during the second cycle, which means that further treatments might not cause significant damage or structural changes in this material.

Fig. 10 presents the cross sections of the samples after the elastic modulus experiments. The higher decarbonized area and apparent porosity of the 10C sample resulted in similar values of E after two thermal treatments, when compared with 10SBC composition. Nevertheless, the addition of the antioxidant blend comprised by sodium borosilicate glass, Si, and boron carbide provided a better carbon protection in the evaluated castable samples.

4. Conclusions

Ultrasonic measurements using the long bar mode were able to identify the temperature range where the mechanisms of cracks healing (during heating) and opening (during cooling) were effective. Castable 10SBC presented the highest elastic modulus during heating due to the antioxidant blend performance (Si, B_4C and sodium borosilicate glass) in an oxidizing atmosphere.

The low E values of the 10C and 10SBC castables measured at the beginning of the first heating cycle are associated with the carbon content, the flaws generated during the castables preparation, and the decomposition of the hydrated phases contained in the refractory samples. The progressive elastic modulus increase with temperature is related to the micro-

Table 3
Information of the transformation observed along the elastic modulus evaluation.

Composition		Hysteresis area (GPa °C)
1° cycle	10SBC	80.454
	10C	34.618
2° cycle	10SBC	17.553
	10C	18.086

structural transformations, such as B_2O_3 and $(Al_2O_3)_9(B_2O_3)$ formation, and sintering.

The use of the FactSage software and the thermodynamic calculations provided useful data which enabled the understanding and prediction of phase changes; and allowed one to estimate the viscosity of the liquid formed in the refractory castables as temperature increased. Additionally, the decrease in the liquid viscosity, mullite formation and carbon oxidation affected the rigidity of the samples at high temperatures. During initial high temperature cooling, the increase in E is related to the usual stiffening of the material when temperature decreased due to an increase in the liquid viscosity. As the castables continued to cool, the residual stresses imposed by the thermal expansion mismatch generated microcracks in the 10C and 10SBC castables' microstructure, leading to lower E values.

The 10SBC refractory showed the lowest hysteresis area during the second cycle, which means that further treatments might not cause significant damage or structural changes in this material. However, due to the action of three antioxidants added to the sample, this composition presented significant changes in the elastic modulus profile during its first thermal treatment.

It must be pointed out that the elastic modulus evolution of the refractory castables as a function of the temperature (for samples attained after curing and drying steps) provides very useful information, enabling one to identify the main microstructural transformations of these complex compositions, and provides valuable inputs for the thermo-mechanical computing simulation. Besides the scientific aspect, these results are relevant to the structural design of the castables, as well as to detecting the critical temperature ranges during material use.

Acknowledgements

The authors are grateful to the Brazilian research funding institution FAPESP, FIRE (Federation for International Refractory Research and Education), the École Nationale Supérieure de Céramique Industrielle (ENSCI – Limoges – FR), and Magnesita Refratários S.A. for the financial support of this work.

References

[1] J.M. Auvray, C. Gault, M. Huger, Evolution of elastic properties and microstructural changes versus temperature in bonding phases of alumina and alumina–magnesia refractory castables, J. Eur. Ceram. Soc. 27 (2007) 3489–3496.

[2] E. Nonnet, N. Lequeux, P. Boch, Elastic properties of high alumina cement castables from room temperature to 1600 °C, J. Eur. Ceram. Soc. 19 (1999) 1575–1583.
[3] W.L. Headrick Jr., R.E. Moore, A.V. Leuven, Measuring refractory MOE at high temperatures, Ceram. Ind. (2000) 19–25.
[4] H. Asakura, H. Minamizono, M. Nakatsukasa, Development of static elastic modulus measurement apparatus at elevated temperatures, Shinagawa Technical Report 43 (2000) 83–90.
[5] C. Aksel, The effect of mullite on the mechanical properties and thermal shock behavior of alumina–mullite refractory materials, Ceram. Int. 29 (2003) 183–188.
[6] F. Nazaret, H. Marzagui, T. Cutard, Influence of the mechanical specificities of damaged refractory castables on the Young's modulus determination, J. Eur. Ceram. Soc. 26 (2006) 1429–1438.
[7] H. Baudson, F. Debucquoy, M. Huger, C. Gault, M. Rigaud, Ultrasonic measurement of Young's modulus MgO/C refractories at high temperature, J. Eur. Ceram. Soc. 19 (1999) 1895–1901.
[8] E.Y. Fogaing, M. Huger, C. Gault, Elastic properties and microstructure: study of two fused cast refractory materials, J. Eur. Ceram. Soc. 27 (2007) 1843–1848.
[9] M. Dimitrijevic, M. Posarac, J. Majstorovic, T. Volkov-Husovic, B. Matovic, Behavior of silicon carbide/cordierite composite material after cyclic thermal shock, Ceram. Int. 35 (2009) 1077–1081.
[10] T. Chotard, J. Soro, H. Lemercier, M. Huger, C. Gault, High temperature characterization of cordierite–mullite refractory by ultrasonic means, J. Eur. Ceram. Soc. 28 (2008) 2129–2135.
[11] N. Tessier-Doyen, Étude experimentale et numerique du comportement thermomecanique de materiaux refractaires modeles, Thesis – Université de Limoges, 2003.
[12] D.N. Boccaccini, M. Romagnoli, E. Kamseu, P. Veronesi, C. Leonelli, G.C. Pellacani, Determination of thermal shock resistance in refractory materials by ultrasonic pulse velocity measurement, J. Eur. Ceram. Soc. 27 (2007) 1859–1863.
[13] N. Tessier-Doyen, M. Huger, J.C. Glandus, Experimental study of the elastic behavior of model refractory materials, in: Proceedings of the Advances in Refractories for the Metallurgical Industries – 4th International Symposium, 2004, pp. 889–902.
[14] Y. Jollif, M. Huger, J.C. Glandus, Experimental and numerical study of the elastic modulus vs temperature of debonded model materials, Comput. Mater. Sci. 44 (2009) 826–831.
[15] M. Huger, D. Fargeot, C. Gault, High temperature measurement of ultrasonic wave velocity in refractory materials, High Temp. High Press. 34 (2002) 193–201.
[16] M. Huger, Oxydation et endommagement d'origine thermoque, evalués par techniques ultrasonores à haute temperature de composites SiC/C/SiC non protégés, Thesis – Université de Limoges, 1992.
[17] A.P. Luz, F.A.O. Valenzuela, V.G. Domiciano, M.A.M. Brito, V.C. Pandolfelli, Improved oxidation resistance of high-carbon-containing castables via antioxidant blend, Am. Ceram. Soc. Bull. 88 (2009) 40–46.
[18] R.G. Pileggi, A.E. Paiva, J. Gallo, V.C. Pandolfelli, A novel rheometer for refractory castables, Am. Ceram. Soc. Bull. 79 (1) (2000) 54–58.
[19] B. Rand, B. McEnaney, Carbon binders from polymeric resins and pitch. Part I – pyrolysis behavior and structure of the carbons, Br. Ceram. Trans. J. 84 (1985) 157–165.
[20] I.R. Oliveira, V.C. Pandolfelli, Refractory castables prepared with hydratable alumina: the dispersant effect, Cerâmica 55 (2009) 33–39 (in Portuguese).
[21] A.P. Luz, F.A.O. Valenzuela, V.G. Domiciano, M.A.M. Brito, V.C. Pandolfelli, Thermo-mechanical–chemical characterization of high-carbon-containing refractory castables, J. Tech. Assoc. Refract., Jpn. 29 (2) (2009) 3–7.
[22] S. Wu, N. Claussen, Reaction bonding and mechanical properties of mullite/silicon carbide composites, J. Am. Ceram. Soc. 77 (11) (1994) 2898–2904.
[23] G.J. Browning, G.W. Bryant, H.J. Hurst, J.A. Lucas, T.F. Wall, An empirical method for the prediction of coal ash slag viscosity, Energy Fuels 17 (3) (2003) 731–737.
[24] A. Nishikawa, Technology of Monolithic Refractories, Plibrico Japan Company Limited, Tokyo, 1984.
[25] C. Pascoal, V.C. Pandolfelli, Refractory bauxites: chemical composition, phases and properties – Part II, Cerâmica 46 (2000) 131–138 (in Portuguese).
[26] G. Briche, N. Tessier-Doyen, M. Huger, T. Chotard, Investigation of the damage behaviour of refractory model materials at high temperature by combined pulse echography and acoustic emission techniques, J. Eur. Ceram. Soc. 28 (2008) 2835–2843.